ChemPlusChem

Research Article
doi.org/10.1002/cplu.202400005

Chemistry Europe
European Chemical Societies Publishing

www.chempluschem.org

Highly Efficient and Reproducible Sonochemical Synthesis of ZnO Nanocrystals

Ambra Fioravanti,*[a] Mauro Mazzocchi,[b] Pietro Marani,[a] Francesca Pedrielli,[a] Maria Cristina Carotta,[a] Michele Sacerdoti,[c] Maria Carmen Valsania,[d] and Sara Morandi*[d]

Sonochemical synthesis can be a facile, fast, efficient, versatile and economical way to prepare a large variety of conventional or novel nanostructured materials (metallic, magnetic, semiconducting, polymeric, etc.). In this work, zinc oxide nanocrystals were synthesized by irradiating and heating at 90 °C in a commercial ultrasonic bath a water solution of zinc nitrate hexahydrate and ammonia solution or hexamethylenetetramine as base catalysts. The evolution of the powder morphology and its crystalline structure were investigated at different times of ultrasonic irradiation (0–9 hours) and compared with those of samples obtained by only heating the solutions in a muffle furnace in order to enlighten the growth mechanism. It resulted that: i) the crystal morphology depends on the selected base, ii) for samples obtained by using ultrasounds, the homogeneity of the powders depends on the irradiation time, iii) by comparing all samples obtained at 7 hours of heating, the aspect ratio of the crystals is higher for those that also underwent to ultrasounds.

Introduction

Zinc oxide (ZnO) is one of the most studied, synthesized and attractive material both in research and industrial areas. The reason is certainly the wide range of intrinsic properties combined with its aptitude for being easily grown in different structures and nanostructures, increasing even more the variety of its functional properties.[1] It is a direct wide band-gap (3.37 eV) semiconductor with n-type conductivity due to intrinsic stoichiometric defects, generally oxygen vacancies, and it has a high exciton binding energy of 60 meV, ensuring both an efficient excitonic emission and an ultraviolet luminescence at room temperature (RT). ZnO is also transparent to visible light and can be obtained with high conductivity by doping.[2,3] Its common and stable phase at ambient conditions is hexagonal wurtzite, which consists of alternating planes of O^{2-} and Zn^{2+} ions tetrahedrally coordinated, stacked alternately along the polar c-axis. The tetrahedral coordination in ZnO results in non-centrosymmetric structure giving to zinc oxide also piezoelectric and pyroelectric properties.[4] It is characterized by a non-toxic nature, antibacterial properties, and generally low-cost production at relatively low temperatures.[5]

Additionally, it can be prepared by exploiting several physical and chemical methods,[6–8] obtaining a large family of 0, 1, 2 or 3-dimensional structures. Consequently, besides the conventional applications, novel ones resulted in optoelectronics, hybrid solar cells, sensors, biomedical field, foods, but it is also broadly used as an additive in several materials or products (plastics, ceramics, glass, cement, lubricants, paints, etc.).[9–13]

Over the last few decades, several studies were performed with the aim to control the morphology during crystal growth, confirming its strict correlation with the material final properties.[14] At the same time, a great interest in exploring new synthesis methods to prepare nanomaterials is documented, for example by using hydro or solvo-thermal synthesis,[8] microwave[15] and/or ultrasonic assisted routes.[16] The last mentioned preparation technique, also known as sonochemical synthesis, takes advantage to apply high intensity ultrasounds to the synthesis solution. The ultrasonic waves (frequency range 20 kHz–15 MHz) do not directly interact with chemical species, but generate acoustic cavitation in the liquid. This process involves the formation, the growth and the fast (few μs) implosive collapse of bubbles in the liquid, producing rapidly and locally extreme temperature and pressure conditions followed by a fast cooling. Therefore, the collapse of bubbles promotes high velocity inter-particle collisions, which can be used in material synthesis.[17–19] In the literature, many sonochemical syntheses were reported and successfully carried out obtaining a multitude of different single and compound materials,[20] including ZnO.[21] Various works reported ZnO sonochemical synthesis, in which the commonly used zinc precursors were zinc nitrate hexahydrate, zinc chloride, and zinc acetate dihydrate. As base catalysts to obtain alkaline environ-

[a] A. Fioravanti, P. Marani, F. Pedrielli, M. C. Carotta
Institute of Sciences and Technologies for Sustainable Energy and Mobility (STEMS)
National Research Council (CNR)
Via Canal Bianco, 28, 44124, Ferrara, Italy
E-mail: ambra.fioravanti@stems.cnr.it

[b] M. Mazzocchi
Institute of Science, Technology and Sustainability for Ceramics (ISSMC)
National Research Council (CNR)
Via Granarolo, 64, 48018, Faenza, Italy

[c] M. Sacerdoti
Department of Physics and Earth Science
University of Ferrara
Via G. Saragat, 1, 44122, Ferrara, Italy

[d] M. C. Valsania, S. Morandi
Department of Chemistry
University of Turin
Via P. Giuria, 7, 10125, Turin, Italy
E-mail: sara.morandi@unito.it

ment ammonium hydroxide (NH_4OH), sodium hydroxide (NaOH) and hexamethylenetetramine (HMTA) were typically selected. Often, ZnO syntheses were performed with the exploitation of seeds, surfactants and templates.[13,22,23] However, another advantage in sonochemical synthesis is the unnecessary use of seeds, surfactants and templates.[24]

This work aims to investigate the effects of ultrasounds on the ZnO crystallization, growth and morphology without seeds, surfactants and templates addition. The same zinc precursor, zinc nitrate hexahydrate, water as medium and two different base catalysts (NH_4OH or HMTA) were used. Firstly, two ZnO were obtained by heating in a muffle furnace for 7 hours the mixtures at a temperature of 90 °C. The thermal treatment conditions were chosen from literature to obtain directly ZnO without requiring the calcination process.[25,26] Those were made as reference samples with the purpose to compare them with ZnO materials obtained through combined thermal and ultrasonic treatment for which the morphology and crystalline structure were investigated at different treatment times (0–9 hours).

Results and Discussion

For the sake of clarity, the essential information about the samples is summarized in Table 1, while in the experimental section further details on the synthesis procedures and characterizations are described. In the following, the sample names as reported in Table 1 refer to powders obtained with a treatment of 7 hours, whereas in case of different treatment duration, the time is specified after the sample name.

By comparing the yield of the synthesis in which the treatment time was 7 hours, it was observed that it is higher for materials obtained through ammonia solution with respect to those obtained by using HMTA as catalyst. The effect of ultrasounds in both cases increased the yield, in particular for HMTA synthesis, for which it resulted almost doubled. The Specific Surface Areas (SSAs) of the samples were similar, with a value slightly higher for ZnO_1HU. Figure 1 shows the morphology of ZnO_1H and ZnO_2H powders.

In both cases, the materials appear as a series of micro-crystals with hexagonal section. The homogeneity in shape and dimension was better for ZnO_1H, in which there is a predominance of single crystals and only few aggregates in flower structure. The opposite situation is evident for ZnO_2H sample, in which crystals with different dimensions mainly aggregate in flower structure. For ZnO_1H the average length of micro-crystals is about 5 μm and the average diameter about 300 nm, thus a mean aspect ratio of 17. In ZnO_2H, the micro-crystals have an average length of about 2 μm and an average diameter of about 400 nm, thus a mean aspect ratio of 5. Furthermore, only the hexagonal micro-crystals in ZnO_1H end with pyramidal tip at both sides. This is related to a rapid depletion of Zn ions, leading to the formation of incomplete structures with a needle-like tips.[27] In Figure 2 and 3 SEM images (indicated as 7 hours) of the samples prepared in ultrasonic bath from the same synthesis with NH_4OH and HMTA, respectively, are shown. Additionally, these figures contain the images of the powders at progressive time of sonication, from 0 to 9 hours.

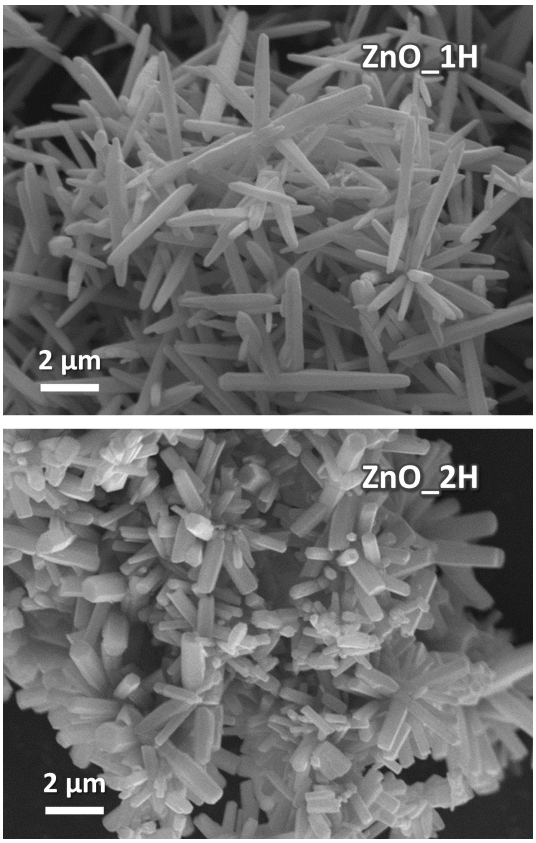

Figure 1. SEM images of ZnO_1H and ZnO_2H, obtained in muffle furnace.

It has to be reported that, only after the addition of NH_4OH, the transparent solution containing zinc nitrate hexahydrate becomes cloudy. The first image of Figure 2 shows the morphology of solid ZnO precursor that forms almost immedi-

Table 1. Sample name and basic information: base used, instrument in which samples are treated, treatment time, yield of the synthesis and Specific Surface Area (SSA) of the powders.

Sample name	Base	Treat.at 90 °C in	Treat. time (h)	Yield %	SSA (m^2/g)
ZnO_1H	NH_4OH	Muffle furnace	7	90	11.4
ZnO_1HU	NH_4OH	Ultrasonic bath	7	94	13.3
ZnO_2H	HMTA	Muffle furnace	7	30	11.0
ZnO_2HU	HMTA	Ultrasonic bath	7	55	10.9

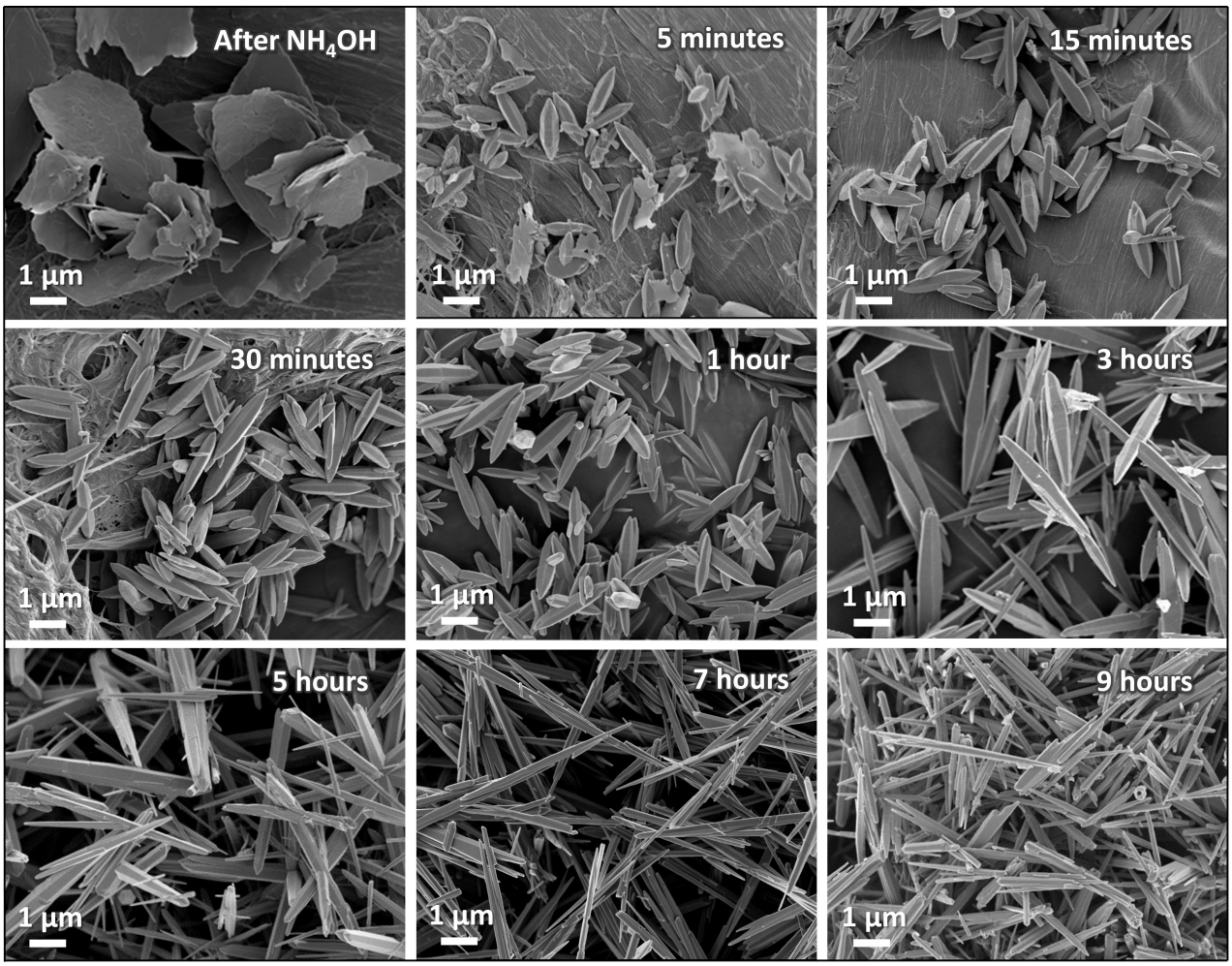

Figure 2. SEM images for the synthesis with NH_4OH at different sonication time, from 0 to 9 hours.

ately after the addition of NH_4OH at RT and therefore before ultrasonic treatment. The pH rapidly reached the value of 10.5, due to the quick dissolution of NH_4OH that makes available the hydroxide ions. In particular, the material is made of rhombic sheets with diagonals of few μm, a crystalline habit consistent with that of ε-$Zn(OH)_2$. After 5 minutes of ultrasonic treatment at 90 °C (second image of Figure 2), the number and dimensions of sheets decrease and small needles with hexagonal section appear. This suggests a partial dissolution of ε-$Zn(OH)_2$, which becomes complete after 15 minutes (third image of Figure 2), and a direct crystallization of ZnO needles, i.e. one of ZnO characteristic shapes.[27] In the case of HMTA addition at RT (pH of 7.5), the solution starts to become cloudy and a white precipitate begins to form only after 10 minutes in ultrasonic bath at 90 °C. As observed by Matheson, the thermal decomposition of HMTA into formaldehyde and ammonium hydroxide occurs as the solution temperature increases.[28,29] The second image of Figure 3 shows the morphology of the precipitate: micro-crystals not homogeneous in size, but with hexagonal section, suggesting a direct precipitation of ZnO. No other structures are displayed in the image, indicating no extra solid phases. Looking at the crystals shown in SEM images of Figure 2 and 3 for samples at 15 minutes of sonication, a sharp discontinuity in the central region of the crystals is evident. For both materials, the study of the morphology evolution at increasing sonication times leads to the following results: i) there is no formation of crystal aggregates, for example in flower structure, irrespective to the sonication time and base; ii) the shape homogeneity of the powders increases with sonication time: iii) the aspect ratio of the crystals increases with sonication time due to a simultaneous lengthening and width reduction; iv) the sonication time of 7 hours yields the best shape homogeneity and the highest aspect ratio. These observations are in agreement with previous findings which showed that: i) for short sonication times, solutions and precipitants are not mixed uniformly and the generated crystals from the solution are irregularly shaped and of various sizes; ii) as sonication time increases, crystal sizes decrease and become more uniform; iii) prolonged sonication time improves mixing and prevents crystals from aggregating.[19]

Looking at the crystal sizes more in details, for ZnO_1HU the average length of micro-crystals is about 6 μm and the average diameter about 150 nm, thus a mean aspect ratio of 40. In this synthesis, the average sizes of the starting crystals are

Research Article
doi.org/10.1002/cplu.202400005
Chemistry Europe
European Chemical Societies Publishing

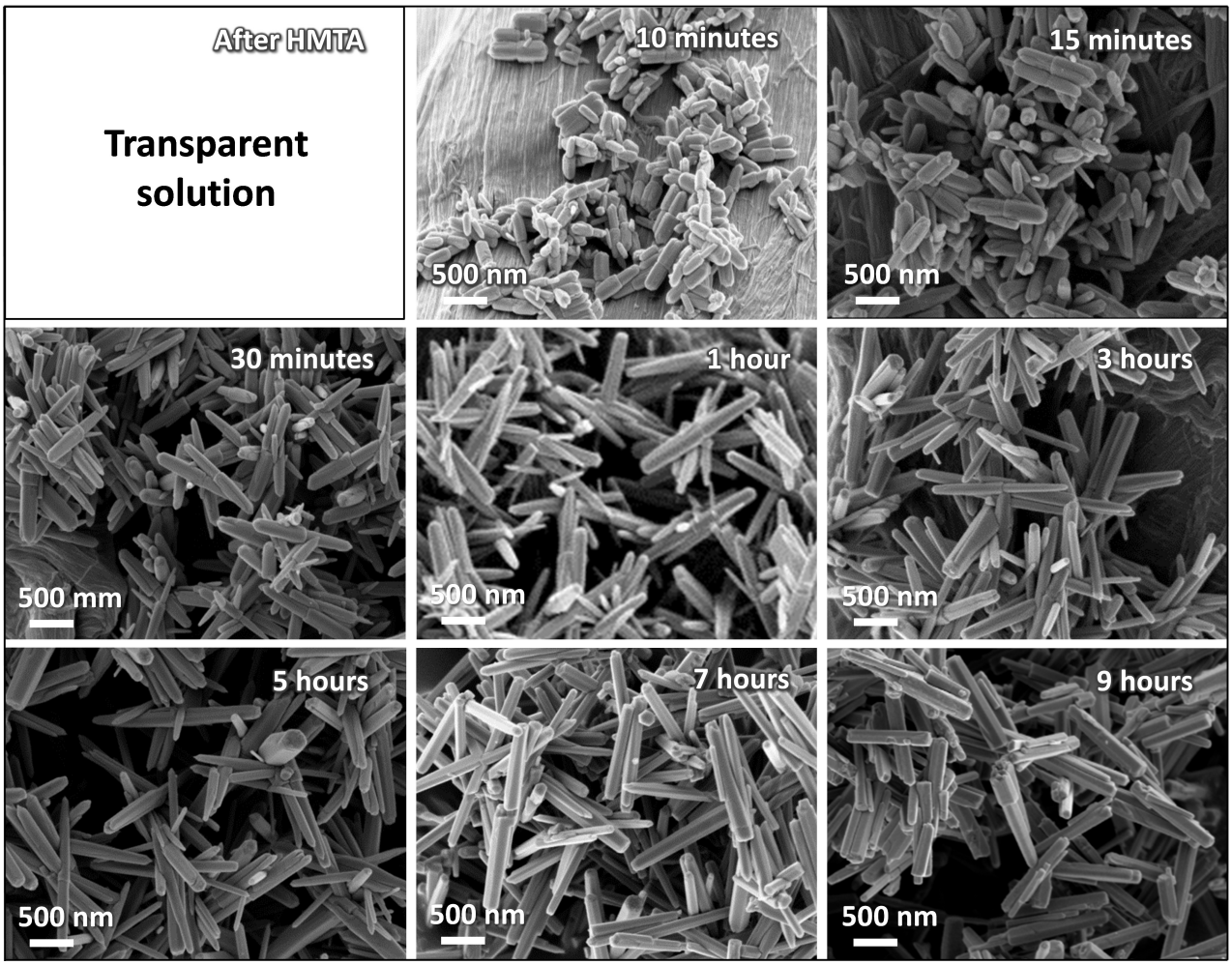

Figure 3. SEM images for the synthesis with HMTA at different sonication time, from 0 to 9 hours.

1.5 μm and 500 nm with aspect ratio of 3. In ZnO_2HU, the micro-crystals show an average length of about 2 μm and an average diameter of about 100 nm, thus a mean aspect ratio of 20. In this synthesis, the average sizes of the starting crystals are 1 μm and 200 nm with aspect ratio of 5. Focusing the attention on ZnO_1HU (SEM image in Figure 2) the pyramidal tips are appreciably longer than those of ZnO_1H (Figure 1). By comparing the crystal shape as a function of the used base, it can be noted that also in the case of ultrasound irradiation, the NH_4OH promotes the growth of needles with hexagonal section and HMTA of hexagonal prisms. Despite the increasing number of research works devoted to understand the role of HMTA in the ZnO synthesis, the debate is still open. Among the proposed roles,[28,30–32] in this case it is reasonable to assign to HMTA the role of OH^- source.

Finally, considering the samples at 9 hours of ultrasonic treatment, the homogeneity decreases and a partial fragmentation of the crystals becomes evident. This could be due to collisions between crystals and/or interaction between shock-waves and crystals (sonofragmentation) as described by Kim and Suslick.[19]

The values of unit cell parameters and the crystallite sizes obtained from the XRD patterns of the four compared powders are reported in Figure 4 and Table 2, respectively. XRD analysis showed a hexagonal wurtzite structure (space group $P6_3mc$)

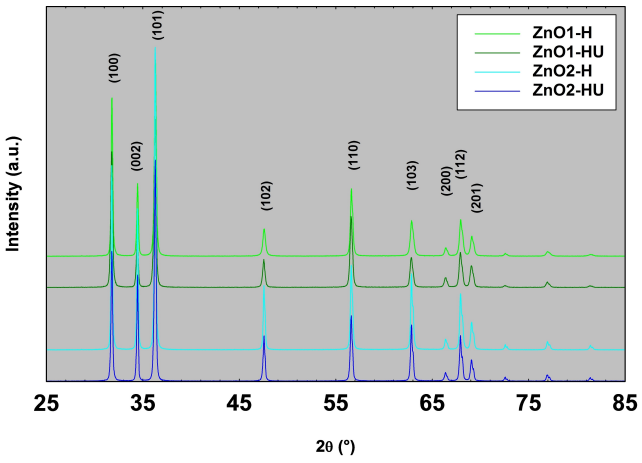

Figure 4. XRD patterns of the four ZnO samples.

Table 2. Values of unit cell parameters (a, c, and volume Vol., Bragg R factor R_B) and crystallite size (C.S.) calculated with Williamson-Hall method. The estimated standard deviations are reported in parentheses and they refer to the last digit of the value.

Sample	a (Å)	c (Å)	Vol. (Å^3)	R_B	C.S. (nm)
ZnO_1H	3.25013(3)	5.20792(7)	47.641(1)	2.23	51
ZnO_1HU	3.25079(2)	5.20911(6)	47.672(1)	2.72	40
ZnO_2H	3.24989(2)	5.20621(5)	47.619(1)	2.81	52
ZnO_2HU	3.25061(3)	5.20774(6)	47.654(1)	3.42	53
JCPDS No. 36–1451	3.249	5.206	47.62	–	–

irrespective of the synthesis procedure and in good agreement with the ZnO standard (JCPDS, card No. 36–1451). No extraneous peaks in the diffraction patterns were recorded; therefore, no other crystalline phases are present in any sample. The crystallite sizes are similar in all samples except for ZnO_1HU, which is 10 nm lower, in agreement with SSA values. Taking into account peaks (100) and (002) singularly and applying the Scherrer's equation,[33] it comes out that the crystallites in samples grown in muffle furnace have the same size in the two normal directions. Differently, in samples prepared by ultrasounds irradiation the crystallites are more extended in the direction normal to (002) plane to form platelets with hexagonal base.

XRD analysis performed on ZnO_1HU – 1 hour and ZnO_2HU – 1 hour confirmed only ZnO phase with hexagonal wurtzite structure. Furthermore, also the crystalline phase of solid ZnO precursor after the addition of NH_4OH at RT before the ultrasound irradiation was investigated confirming that it corresponds to zinc hydroxide ε-$Zn(OH)_2$ with orthorhombic structure, space group $P2_12_12_1$, as expected.

To better understand the growth mechanism of ZnO mediated by the ultrasounds at early stages, TEM analysis was performed on samples after 15 minutes of treatment. As example, in Figure 5 TEM and high resolution (HR)-TEM images of the sample ZnO_2HU–15 minutes are reported. In Figure 5B the planes normal to [001] direction are clearly observable. TEM analysis confirms the direct crystallization of ZnO in the solution containing HMTA and precipitation of ZnO after dissolution of ε-$Zn(OH)_2$ when NH_4OH was used. Additionally, HR-TEM micrographs allow to observe the crystalline planes in the central region of crystals after 15 minutes of ultrasound treatment. As reported above, in this region there is a visible morphological discontinuity (see SEM images in Figure 2 and 3), but crystalline planes shown by HR-TEM image (see as example Figure 5B) put in evidence no lattice discontinuity and no structural defects. This could be explained by considering a normal twinning,[34] involving the plane $(000\bar{1})$ already reported in Dana's Series of Mineralogies.[35]

Taking into account the above discussed results and the chemical reactions to form ZnO in alkaline environment reported by Xu and Wang,[36] it is possible to describe the growth mechanisms of the obtained powders:

$$Zn^{2+} + 2OH^- \rightleftharpoons Zn(OH)_2 \quad (1)$$

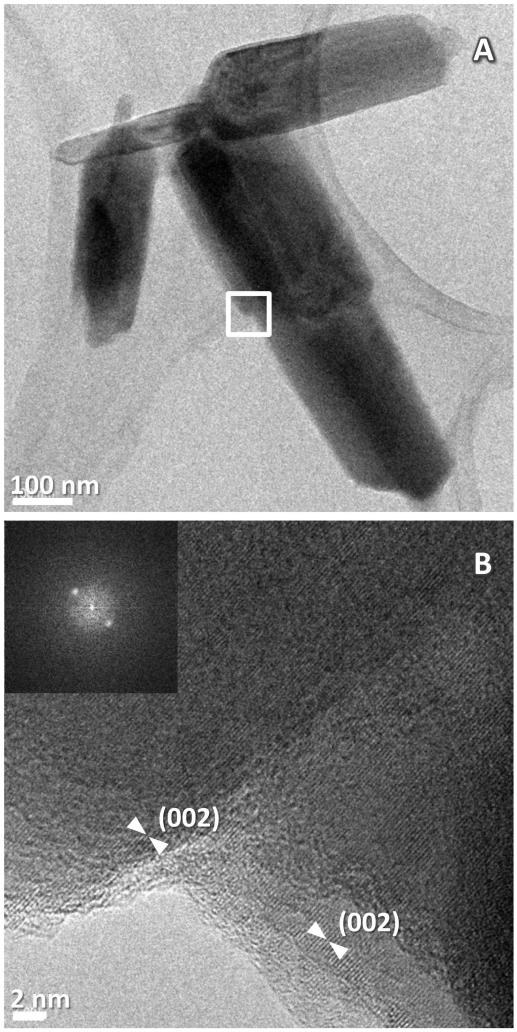

Figure 5. TEM (A) and HR-TEM (B) images of the sample ZnO_2HU – 15 minutes (instrumental magnification: 25 and 600 kX, respectively). Image B shows the central region of the crystal.

$$Zn(OH)_2 + 2OH^- \rightleftharpoons [Zn(OH)_4]^{2-} \quad (2)$$

$$[Zn(OH)_4]^{2-} \rightleftharpoons ZnO_2{}^{2-} + 2H_2O \quad (3)$$

$$ZnO_2{}^{2-} + H_2O \rightleftharpoons ZnO + 2OH^- \quad (4)$$

In the syntheses performed in the present study, $Zn(NO_3)_2$*$6H_2O$ provides Zn^{2+} ions, while bases NH_4OH and HMTA are the source of OH^- ions. The interaction between these ions

causes zinc hydroxide precipitation, while successive transformation to zinc oxide could follow two processes: i) ZnO precipitation after the dissolutions of ε-$Zn(OH)_2$ or ii) the direct in situ crystallization of ZnO (i.e. phase transition). The predominant mechanism influences the morphology and depends on the solution pH and other growth conditions. In general, at low pH value ε-$Zn(OH)_2$ does not dissolve and the predominant mechanism is direct phase transition, whereas at high pH value ε-$Zn(OH)_2$ dissolves with a subsequent ZnO precipitation.[27] The last is clearly the case of synthesis with NH_4OH, for which the formation of ε-$Zn(OH)_2$ and its consecutive dissolution boosted by temperature and ultrasounds together with ZnO precipitation was observed.

From the morphological and structural characterizations, it can be supposed that hexagonal platelets are the initial growth crystalline units, according to observations by Katarapu et al..[25] Crystallite, after nucleation, usually develops into a macroscopic crystal with well-defined crystallographic faces which are related to different crystal planes that generally show differences in growth rate. In ZnO, Laudise[37] firstly observed the relationship between growth rates in different directions that is: $v_{[0001]} > v_{[01\bar{1}\bar{1}]} > v_{[01\bar{1}0]} > v_{[01\bar{1}1]} > v_{[000\bar{1}]}$. The higher the growth rate, the more energetically favored the growth in the related direction. In ZnO, vertical growth represents the preferential growth direction, which it is responsible of the most probable rod shapes. Moreover, it is reasonable to associate the presence of pyramid terminations (NH_4OH) to a faster growth with respect to that of prismatic shape (HMTA). Considering the growth rates, in particular those related to preferential direction $v_{[0001]} > v_{[000\bar{1}]}$, the expected ends in a ZnO crystal should be a pyramid and a pyramid with pedial termination.[38] For prepared powders with needle shape the crystal terminations are two similar pyramids, confirming the presence of a normal twinning, involving the plane $(000\bar{1})$, in the middle region of the crystal, as mentioned above.

After the acceleration of nucleation and growth, at the increase of treatment time ultrasounds promote erosion of the crystal surface, producing other crystal units available for further growth of the crystals, but in the preferred direction: this explains increasing aspect ratio in crystals from 0 to 7 hours.

Conclusions

Four zinc oxide nanocrystalline samples were successfully synthesized without calcination directly by heating at 90 °C, or by heating at 90 °C and irradiating in a commercial ultrasonic bath an aqueous solution containing zinc nitrate hexahydrate and a weak base. The evolution of the powder morphology and its crystalline structure were investigated at different times of ultrasonic irradiation (0–9 hours) and compared with samples obtained only by heating the solutions in a muffle furnace allowing highlighting the effect of ultrasound and understanding the growth mechanism. The main results are: i) the crystal morphology depends on the base, ii) for samples obtained by using ultrasounds the homogeneity of powders depends on time of irradiation, iii) use of ultrasounds avoids crystal aggregation, iv) by comparing all samples obtained at 7 hours of heating, the aspect ratio is higher for those which also underwent to ultrasounds.

The ZnO nanocrystal sonochemical synthesis resulted easy, highly efficient, economic and reproducible, making it an industrially viable solution. Furthermore, by changing the sonication time, the size and aspect ratio of the crystals could be tuned. Therefore, it certainly represents an advantageous way to prepare ZnO or ZnO based materials and it can be convenient also for the preparation of other oxide nanopowders.

Experimental Section

Four ZnO powders were obtained from the slight adjusting of ZnO synthesis described in previous papers.[6,26] All syntheses started by dissolving zinc nitrate hexahydrate $Zn(NO_3)_2{*}6H_2O$,(> 99.0 % Sigma-Aldrich) in deionized water. A weak base dissolved in water solution was then added to catalyze hydrolysis at room temperature. In case of ammonium hydroxide (NH_4OH water solution, Carlo Erba Reagents) the solution reached the pH of 10, for hexametilenetetramine (HMTA, Sigma-Aldrich) the solution pH was 7.5. Mixtures were then treated at 90 °C measured in muffle furnace (Lenton) for 7 hours or in a commercial ultrasonic bath (37 KHz, Elmasonic S120H) up to 9 hours. Powders were filtered by gravity, washed several times with deionized water and dried at 70 °C for 8 hours in oven. The yields reported in Table 1 represent average yields calculated on eight syntheses for each sample. The SSAs were evaluated by applying the Brunauer—Emmett–Teller (BET) method to adsorption/desorption isotherms of N_2 at −196 °C obtained with a Micromeritics ASAP 2010 physisorption analyzer. Morphological characterization of the samples was performed by Field Emission Scanning Electron Microscopy (FE-SEM) using a Carl Zeiss Sigma microscope working at 3.00 kV. Due to the small amount of crystallized material at early stages of growth in sonicated solutions, the samples were collected on a filter paper directly dipped into the mixture. Moreover, a High Resolution Transmission Electron Microscope (HR-TEM) model Jeol JEM 3010 (300 kV) equipped with a LaB_6 filament was used to examine crystalline planes arrangement in the central region of the samples at 15 minutes of sonication treatment. Samples were deposited on a copper grid, coated with a porous carbon film. Digital micrographs were acquired by an Ultrascan 1000 camera and the images processed by Gatan digital micrograph. Crystalline structures were evaluated through Rietveld analysis of X-ray diffraction (XRD) patterns collected over the range $2\theta = 10°–100°$, with steps of 0.02° and 2 s of dwell time obtained with a Bruker D8 Advance diffractometer (Cu K radiation, 40 kV, 40 mA). FullProf (release 2021) is the software used for Rietveld analysis.[39] Average crystallite sizes (C.S.) were calculated with the Williamson-Hall method[40] and reported in Table 2, while Scherrer's equation was used to evaluate crystallite dimensions along specific crystallographic directions in particular those related to the peaks (100) and (002).

Conflict of Interests

The authors declare no conflict of interest.

Data Availability Statement

The data that support the findings of this study are available from the corresponding author upon reasonable request.

Keywords: sonochemical synthesis · ultrasounds · sonofragmentation · zinc oxide nanostructures · crystal growth

[1] Z. L. Wang, *Mater. Today* **2004**, *7*, 26–33.
[2] D. K. Sharma, S. Shukla, K. K. Sharma, V. Kumar, *Mater. Today: Proc.* **2020**, *49*, 3028–3035.
[3] A. Janotti, C. G. Van De Walle, *Rep. Prog. Phys.* **2009**, *72*, DOI 10.1088/0034-4885/72/12/126501.
[4] S. Goel, B. Kumar, *J. Alloys Compd.* **2020**, *816*, 152491.
[5] Ü. Özgür, Y. I. Alivov, C. Liu, A. Teke, M. A. Reshchikov, S. Doğan, V. Avrutin, S. J. Cho, H. Morko¸, *J. Appl. Phys.* **2005**, DOI 10.1063/1.1992666.
[6] R. Kumar, Kamakshi, *Synthesis Routes of ZnO Nanocrystallites*, INC, **2021**.
[7] S. Borbón, S. Lugo, I. López, *Mater. Sci. Semicond. Process.* **2019**, *91*, 310–315.
[8] A. Kolodziejczak-Radzimska, T. Jesionowski, *Materials (Basel).* **2014**, *7*, 2833–2881.
[9] M. Waqas, Y. Hui, L. Wang, F. Fan, K. Mahmood, W. Chen, D. H. Chen, Y. Fan, G. Yasmeen, *ChemPlusChem* **2023**, *88*, DOI 10.1002/cplu.202300065.
[10] L. Zheng, Y. Zheng, C. Chen, Y. Zhan, X. Lin, Q. Zheng, K. Wei, *ChemPlusChem* **2012**, *77*, 217–223.
[11] A. G. Păun, S. Popescu, C. Ungureanu, R. Trusca, C. Pirvu, *ChemPlusChem* **2023**, DOI 10.1002/cplu.202300450.
[12] P. K. Vabbina, A. Kaushik, N. Pokhrel, S. Bhansali, N. Pala, *Biosens. Bioelectron.* **2015**, *63*, 124–130.
[13] E. Oh, H. Y. Choi, S. H. Jung, S. Cho, J. C. Kim, K. H. Lee, S. W. Kang, J. Kim, J. Y. Yun, S. H. Jeong, *Sens. Actuators B* **2009**, *141*, 239–243.
[14] A. Hezam, K. Namratha, Q. A. Drmosh, B. N. Chandrashekar, K. K. Sadasivuni, Z. H. Yamani, C. Cheng, K. Byrappa, *CrystEngComm* **2017**, 3299–3312.
[15] K. R. Ahammed, M. Ashaduzzaman, S. C. Paul, M. R. Nath, S. Bhowmik, O. Saha, M. M. Rahaman, S. Bhowmik, T. Das Aka, *SN Appl. Sci.* **2020**, *2*, 1–14.
[16] X. L. Hu, Y. J. Zhu, S. W. Wang, *Mater. Chem. Phys.* **2004**, *88*, 421–426.
[17] K. S. Suslick, G. J. Price, *Annu. Rev. Mater. Sci.* **1999**, 295–326.
[18] X. Hangxun, B. W. Zeiger, K. S. Suslick, *Chem. Soc. Rev.* **2013**, *42*, 2555–2567.
[19] H. N. Kim, K. S. Suslick, *Crystals* **2018**, *8*, DOI 10.3390/cryst8070280.
[20] S. Głowniak, B. Szczęśniak, J. Choma, M. Jaroniec, *Molecules* **2023**, *28*, DOI 10.3390/molecules28062639.
[21] S. R. Veerabhadraiah, S. Maji, A. Panneerselvam, *J. Cryst. Growth* **2022**, *579*, 126430.
[22] N. Pokhrel, P. K. Vabbina, N. Pala, *Ultrason. Sonochem.* **2016**, *29*, 104–128.
[23] M. T. Noman, M. Petru, J. Militky`, M. Azeem, M. A. Ashraf, *Materials (Basel).* **2020**, *13*, 14.
[24] R. Wahab, S. G. Ansari, Y. S. Kim, H. K. Seo, H. S. Shin, *Appl. Surf. Sci.* **2007**, *253*, 7622–7626.
[25] V. Katarapu, H. Pant, S. V. Kummari, R. Kurapati, K. Guruvidyathri, V. V. S. S. Srikanth, *ChemistrySelect* **2023**, *8*, DOI 10.1002/slct.202300221.
[26] J. Q. He, J. Yin, D. Liu, L. X. Zhang, F. S. Cai, L. J. Bie, *Sens. Actuators B* **2013**, *182*, 170–175.
[27] V. Gerbreders, M. Krasovska, E. Sledevskis, A. Gerbreders, I. Mihailova, E. Tamanis, A. Ogurcovs, *CrystEngComm* **2020**, *22*, 1346–1358.
[28] E. D. Matheson, Y. Qu, G. Kartopu, M. K. Etherington, G. Zoppi, V. Barrioz, N. S. Beattie, *J. Mater. Sci. Mater. Electron.* **2023**, *34*, 1–13.
[29] M. N. R. Ashfold, R. P. Doherty, N. G. Ndifor-Angwafor, D. J. Riley, Y. Sun, *Thin Solid Films* **2007**, *515*, 8679–8683.
[30] V. Strano, R. G. Urso, M. Scuderi, K. O. Iwu, F. Simone, E. Ciliberto, C. Spinella, S. Mirabella, *J. Phys. Chem. C* **2014**, *118*, 28189–28195.
[31] W. Feng, B. Wang, P. Huang, X. Wang, J. Yu, C. Wang, *Mater. Sci. Semicond. Process.* **2016**, *41*, 462–469.
[32] C. Lausecker, B. Salem, X. Baillin, V. Consonni, *Cryst. Growth Des.* **2023**, *23*, 2941–2950.
[33] U. Holzwarth, N. Gibson, *Nat. Nanotechnol.* **2011**, DOI 10.1038/nnano.2011.145.
[34] P. Uttam, V. Kumar, K. H. Kim, A. Deep, *Mater. Des.* **2020**, *192*, 108752.
[35] M. O. F. Mineralogy, *Nature* **1960**, *185*, 721.
[36] S. Xu, Z. L. Wang, *Nano Res.* **2011**, DOI 10.1007/s12274-011-0160-7.
[37] R. A. Laudise, A. A. Ballman, *J. Phys. Chem.* **1960**, *64*, 688–691.
[38] W. J. Li, E. W. Shi, W. Z. Zhong, Z. W. Yin, *J. Cryst. Growth* **1999**, DOI 10.1016/S0022-0248(99)00076-7.
[39] D. B. Wiles, R. A. Young, *J. Appl. Crystallogr.* **1981**, DOI 10.1107/s0021889881008996.
[40] M. G. Suryanarayana, C.Norton, *X-Ray Diffraction: A Practical Approach*, Springer, New York, **1998**.

Manuscript received: January 2, 2024
Revised manuscript received: March 5, 2024
Accepted manuscript online: March 10, 2024
Version of record online: April 6, 2024